Journal of Marine Research, 62, 611–638, 2004

Journal of
MARINE RESEARCH

Volume 62, Number 5

An experimental study of a mesoscale vortex colliding with topography of varying geometry in a rotating fluid

by Claudia Adduce[1] and Claudia Cenedese[2,3]

ABSTRACT

The interaction of a self-propagating barotropic cyclonic vortex with an obstacle has been investigated and the conditions for a vortex to bifurcate into two vortices determined. As in a previous study, after a self-propagating cyclonic vortex came into contact with the obstacle, fluid peeled off the outer edge of the vortex and a so-called "streamer" went around the obstacle in a counterclockwise direction. Under certain conditions, this fluid formed a new cyclonic vortex in the wake of the obstacle, causing bifurcation of the original vortex into two vortices. In the present study we performed three sets of idealized laboratory experiments with the aim of investigating the importance on the bifurcation mechanism of the obstacle's horizontal cross sectional geometry, the influence of the height of the obstacle, and the importance of the slope of the obstacle sidewalls. The present results suggest that bifurcation occurs only when the obstacle height is equal or larger than 85% of the vortex height and that steep sloping sidewalls do not influence the bifurcation mechanism. In addition, experiments performed using an obstacle with an elliptical horizontal cross section revealed that the relevant parameter governing the occurrence of bifurcation is the length which the "streamer" has to travel around the obstacle, and not the dimension of the obstacle in the direction orthogonal to the motion of the vortex. Collisions of oceanic mesoscale vortices with seamounts often result in major modifications of their structure, having significant impacts on the redistribution of water properties. Observations of a "Meddy" bifurcating after colliding with the Irving Seamount in the Canary Basin show behavior similar to these idealized laboratory experiments. This suggests that these results could be used to explain and predict the outcome of a vortex colliding with seamounts of varying geometry in the ocean.

1. Universita RomaTre, Via Vito Volterra 62, 00146, Rome, Italy.
2. Woods Hole Oceanographic Institution, Woods Hole, Massachusetts, 02543, U.S.A.
3. Corresponding author ***email: ccenedese@whoi.edu***

1. Introduction

Several hydrographic surveys in the Canary Basin of the eastern Atlantic Ocean have shown the presence of warm and salty Mediterranean water within intense subsurface vortices named meddies (Bower *et al.,* 1997; Richardson *et al.,* 2000). Meddies are believed to form primarily near Cape St. Vincent (Bower *et al.,* 1997) and translate westward into the Atlantic where two major topographic features stand in the meddies' paths: the Horseshoe Seamounts and the Great Meteor Seamounts. Most meddies (~90%) have been observed to collide with these major seamounts after a mean life of 1.7 years. The collision often results in a major disruption of the vortical structure (Richardson and Tychensky, 1998; Richardson *et al.,* 2000) and dispersal of the water properties around the location where the collision occurred. Clearly, the effect of meddies colliding with seamounts, with the consequent redistribution of Mediterranean water, is potentially very important when considering the Mediterranean salt tongue in the North Atlantic (Wang and Dewar, 2003). Furthermore, meddies have been occasionally observed to bifurcate[4] after interacting with a seamount (Richardson and Tychensky, 1998; Richardson *et al.,* 2000) hence relocating the Mediterranean water properties into two vortices. The bifurcation of a meddy enhances the redistribution of heat and salt in the North Atlantic basin since a larger number of vortices will correspond to a larger number of dilute trails of warm and salty water present in the basin (Käse and Zenk, 1987) and to a higher possibility of fatal destruction of the vortex structure with consequent dispersal of water properties.

In addition, atmospheric synoptic-scale cyclonic vortices are generated and travel along the storm tracks that move at an approximately constant latitude. These cyclonic systems can encounter major topographic features such as Greenland, the Rocky Mountains and the Scandinavian Mountains in the Northern Hemisphere, and the Andes and the Southern Alps of New Zealand in the Southern Hemisphere. A recent study investigated the evolution of such synoptic-scale vortices impinging upon Greenland (Schwierz and Davies, 2003) and the splitting of a cyclonic vortex can be observed in the time sequence of ECMWF analysis fields from September 20th, 1993 to September 26th, 1993 (see Fig. 12 of Schwierz and Davies, 2003).

Previous studies have mainly investigated vortex dipole interaction with a circular cylinder (Lucas and Rockwell, 1988; Orlandi, 1993; Voropayev and Afanasyev, 1994; Verzicco *et al.,* 1995). Only recently have very few studies focused on the interaction of monopoles with obstacles and the possibility of bifurcation of the original vortex into two or more vortices (Simmons and Nof, 2000; Cenedese, 2002; Dewar, 2002; Herbette *et al.,* 2003; Wang and Dewar, 2003). Simmons and Nof (2000) analyzed the interaction of a monopolar vortex with a thin wall and found that for a zero potential vorticity lens (with a radius r) to split into two equal lenses, the wall length must be at least $1.19r$. The

4. Herein we will use the term "bifurcation" to indicate the outcome of two or more vortices from the interaction of a single vortex with an obstacle. As discussed below, the interaction can cause some of the vortex fluid to move around the obstacle within the boundary layer whose detachment can generate a new vortex.

interaction of a monopole vortex with a right vertical cylinder was investigated by Cenedese (2002), hereafter referred to as C02. Both a self-propagating vortex and one advected by a background uniform flow bifurcated into two vortices upon interaction with the cylinder provided $400 \leq Re \leq 1100$, where Re is the Reynolds number. These values of Re for bifurcation to occur have been established experimentally. This regime corresponds to values of $0.2 \leq R/r \leq 1.0$, for the self-propagating vortex, and $0.2 \leq R/r \leq 1.3$, for the vortex advected by a background flow, where r is the vortex radius and R is the cylinder radius. The interaction of a vortex with a thin wall is different than a vortex interacting with a cylinder; the most striking difference is that in the former case the horizontal scales have different orders of magnitude, but in the latter case they are the same.

In order to better understand the dynamical processes controlling the bifurcation that may occur when a meddy interacts with seafloor topography, and in particular the influence of the topography sloping sidewalls, height and cross sectional geometry, a series of idealized laboratory experiments has been performed. These three foci aim to better understand the importance of the steep seamount side slopes ($\sim$4%); the effect of seamounts of different vertical extension when compared to the meddies vertical extent (about 1000 m with a core depth in the range 1100–1200 m); and finally the effect of sea floor topography having horizontal scales with finite (i.e. not a thin wall like Simmons and Nof (2000)) but different values (i.e. not a circular shape like C02) in different directions, as observed in some locations in the ocean, for example the Hyres seamount (Richardson and Tychensky, 1998).

However, the present paper will not cover and classify all the possible outcomes of a vortex-topography interaction. We will focus on and discuss the dynamical processes that will cause a vortex to split into two or more vortices. This focus, beside being an interesting fluid dynamics problem linked to the classic studies of flow past a bluff body, has been motivated by recent oceanographic observations (Richardson and Tychensky, 1998; Richardson *et al.,* 2000) and the importance of these possible bifurcations on the redistribution of heat and salt in the North Atlantic (Wang and Dewar, 2003). Hence, since the focus is exclusively on the bifurcation processes, we will classify the outcome of a vortex-topography interaction either by it being a bifurcation or not. Nevertheless, we recognize that the outcome of such interaction is more complicated than this simple binary classification and we leave the investigation of all the different possible outcomes (for example that of a vortex to be destroyed by the interaction) to future studies.

The paper is set out as follows: the experimental apparatus is described in Section 2. "Glancing" interactions are discussed in Section 3. Theoretical consideration of the circulation around an elliptical island and the experimental results are presented in Section 4. The results from experiments investigating the topography height and the sloping sidewalls are given in Sections 5 and 6, respectively. Comparisons with observations are presented in Section 7. Finally, the conclusions of the work are discussed in Section 8.

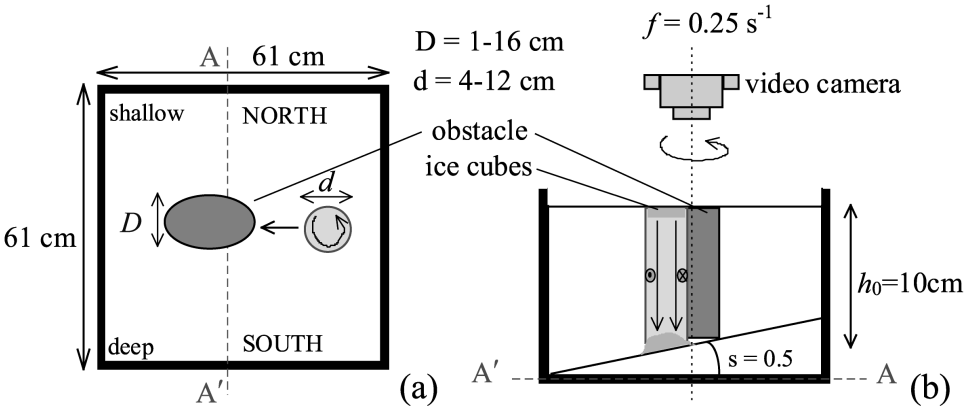

Figure 1. Sketch of the experimental apparatus (not to scale). (a) Top view; (b) side view.

2. Experimental apparatus

The experiments were conducted in a square tank of depth 0.36 m and length and width of 0.61 m. This was mounted concentrically on a 1 m diameter rotating turntable with a vertical axis of rotation. We used a square tank to avoid optical distortion from side views associated with a circular tank. A sketch of the apparatus is shown in Figure 1. The tank had a bottom slope, s, in order for the vortex to self propagate leftward when looking upslope (Cushman-Roisin, 1994; Cenedese and Whitehead, 2000). Although the exact equivalence between the sloping topography and the β plane depends on the smallness of the slope and the Rossby number, we will name for reference North the shallowest part of the tank. Consequently, East is to the right when looking upslope, West is to the left and South is the deepest part of the tank. The tank was filled up to 0.25 m with fresh water, which was initially in solid body rotation. The obstacle was positioned in the central part of the tank, where the water depth was $h_0 = 0.10$ m. The bottom of each obstacle was sliced at an angle so it rested flush with the sloping bottom.

A barotropic cyclonic vortex was generated by placing an ice cube in the water (Whitehead *et al.,* 1990), a method dynamically similar to withdrawing fluid from a sink positioned on the sloping bottom. The vertical velocities, induced by either the sink or the dense plume, induce inward velocities that, in a rotating system, generate a cyclonic vortex. The flexibility in positioning and sizing an ice cube made this method preferred over the sink one. The ice-cube-method forms a dense cold water lens that is confined within a thin bottom Ekman layer. However, the main interest of this paper is the water column spinning cyclonically above the dense water (see C02). The dense plume induces inward velocities along the entire column depth above the bottom lens that are balanced, in order to conserve mass, by radially outward velocities within the bottom dense lens. Since the depth of the dense lens is approximately a tenth of the whole column depth, the outward velocities are ten times larger than the inward velocities. Dense fluid flows radially outward from the bottom dense lens with a very large velocity giving a Rossby number much larger

than unity. Therefore, the dense fluid is not influenced by rotation and does not form an anticyclonic vortex. Instead, the dense fluid moves slowly downslope within the Ekman layer, and veers left (looking upslope) influenced by the Coriolis force. During an initial transition time, lasting approximately one inertial period, the fluid within the dense lens moves downslope together with the whole cyclonic column above it. Influenced by the Coriolis force, the cold lens, together with the cyclonic column above it, veers left and starts drifting westward. The fluid in the cyclonic water column is hydrostatic since vertical velocities have been observed to be negligible when compared to horizontal azimuthal velocities. Furthermore, the addition of dye made Taylor-Column "curtains" visible, implying that the fluid in the column above the dense lens is barotropic. As described above, most of the dense fluid has been observed to leave the dense lens and, with exclusion of the bottom Ekman layer, the whole water depth is occupied by the barotropic cyclonic vortex. Hence, we will assume that the dense fluid on the bottom of the cyclonic column does not influence the dynamics of the vortex-topography interaction. This assumption is supported by experimental observations indicating that the lower dense fluid, upon interaction with the obstacle, does not evolve in a similar manner than the above fluid (i.e. the streamer formation has not been observed to occur in the dense fluid within the Ekman layer). However, we note that, as discussed above, the dense lens influences the dynamics related to the westward propagation of the cyclonic vortex. The above assumptions will allow us to consider the fluid within the vortex to be barotropic and two-dimensional. The diameter of the vortex, $d = 2r$, was ascertained by observations of particle tracks determined to be within the vortex and was varied by changing the size of the ice cube. The azimuthal velocity profile of the vortex is similar to that of a Rankine vortex with an approximately constant relative vorticity (solid body rotation) up to a radius $r' = r'_{\max}$, and then a velocity that decays roughly like $1/r'$, where r' is the radial coordinate originating in the vortex center. We have measured the velocity profile of some representative vortices; however, the vortex radius measurements were done visually for all experiments, looking at the particle tracks as discussed above. The measured vortex radius r does not correspond to $r'_{\max}$, where the vortex azimuthal velocity is maximum, but is located along the $1/r'$ profile, where the velocity has decayed by approximately 30%. The vortex radius measurements were consistent with this velocity decay definition throughout the experiments and also with the measurements conducted by C02.

In order to study the influence of the 3-D obstacle geometry on the bifurcation mechanism, we carried out three sets of experiments. Table 1 illustrates the range of values for the parameters used. First, to investigate the effect of the horizontal cross sectional geometry, we used a cylinder with an elliptical base that extended throughout the entire water depth. The experiments were carried out using two different ellipses and positioning the minor axis of the ellipse both parallel and perpendicular to the direction of propagation of the vortex. Second, to investigate the influence of the height of the obstacle, we carried out a series of experiments with a submerged circular cylinder of diameter $D = 2R$ and whose height, h, was varied. Finally, the importance of the slope of the obstacle sidewalls

Table 1. Range of the values of the parameters varied during the experiments using an elliptical cylinder, a submerged circular cylinder, and a truncated conical obstacle. The following parameters were kept fixed with the following values: $f = 0.25\ s^{-1}$, $s = 0.5$, $\nu = 0.01\ 10^{-6}\ m^2\ s^{-1}$, $h_0 = 0.10$ m. The value of the Rossby number $R_o = \zeta/f$ varied between 0.6 and 1. Finally, a typical value of v_e is 0.005 m s^{-1}. Variables are expressed in MKS units.

	Minor axis	Major axis		D_{eq}	d	Y
Elliptical	0.05	0.12		0.09	0.08:0.12	−0.04:0.06
	0.08	0.16		0.13	0.08:0.12	−0.06:0.06
	h/h_0			D	d	Y
Submerged	$\frac{1}{4}, \frac{1}{2}, \frac{3}{4}, \frac{17}{20}$			0.01:0.09	0.06:0.13	−0.08:0.05
	slope	D_b	D_t	D_{av}	d	Y
Truncated Cone	70°	0.07:0.18	0.006:0.11	0.04:0.15	0.08:0.13	−0.09:0.04
	83°	0.03:0.09	0:0.06	0.02:0.08	0.04:0.13	−0.08:0.06

was investigated in a third set of experiments with truncated conical obstacles having a circular horizontal cross section and extending throughout the entire water depth. Two different slopes of the cone were used (the motivation for this choice is given in Section 6b) and the average diameter, D_{av}, between the top, D_t, and base, D_b, diameters of the cone was varied.

For all the experiments, the Coriolis parameter f was fixed at $0.25\ s^{-1}$ and the bottom slope was set at $s = \tan\alpha = 0.50$, where α is the angle between the sloping bottom and the horizontal. With this choice of slope magnitude the self-propagating vortex was observed to move westward with a speed $U \approx 0.002\ m\ s^{-1}$. The vortex was generated approximately 0.10 m to the left of the right wall (looking upslope) and the obstacle's center, positioned in the middle of the tank, was approximately 0.20 m left from the vortex generation site. Hence, the vortex moved 0.20 m westward and interacted with the obstacle before the spindown time $\tau = h_0/\sqrt{\nu f} = 200$ s. Furthermore, the whole experiment ended when the vortex was approximately 0.10 m from the left wall (looking upslope) so that the wall effects can be ignored and bottom friction can be neglected. This slope magnitude choice does not allow the translation timescale of the vortex $t_d = d/2U$ to be the same as in the real site (ocean $t_d \approx 6.5$ days; laboratory $t_d \approx 0.5$ day, where in the laboratory 1 day $\equiv T = (4\pi/f)$. However, we believe that this should not affect this study, since both in the laboratory and the ocean the eddy reduces its translation velocity drastically in proximity of the seamount (Richardson and Tychensky, 1998). In the present experiments, the value of the Rossby number $R_o = \zeta/f$ varied between 0.6 and 1.

The geometry of the encounter is described by the ratio Y/R (Fig. 2). R is half of the obstacle length orthogonal to the direction of propagation of the vortex, where for the truncated cone, we considered the obstacle length to be equal to D_{av}. Y is defined as the

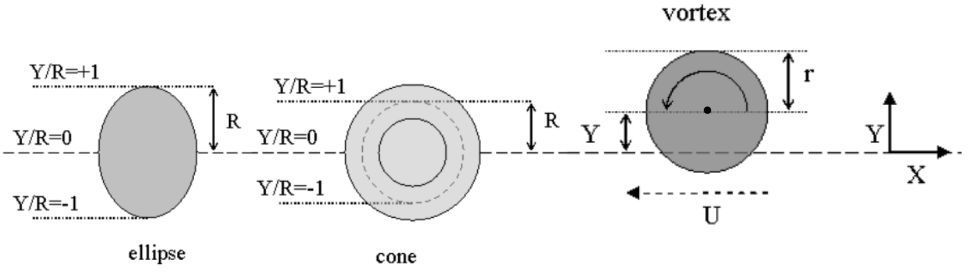

Figure 2. Sketch illustrating the collision between the vortex and different obstacles. The ratio Y/R is a measure of the geometry of the interaction. For $Y/R > 0$ ($Y/R < 0$) the interaction will take place in the northern (southern) side of the obstacle and for $Y/R = 0$ the interaction will be central. The dashed line within the cone represents the circle having a diameter equal to D_{av}.

distance in the y-direction between the center of the vortex and the horizontal line passing through the center of the obstacle in the x-direction. The parameter Y/R was varied between -2.2 and 2.1 and is a measure of the geometry of the interaction in that for $Y/R > 0$, the interaction takes place in the northern side of the obstacle, for $Y/R = 0$, the interaction is central and for $Y/R < 0$, it takes place in the southern side of the obstacle.

A video camera was mounted above the tank and fixed to the turntable in order to observe the flow in the rotating frame. The vortex was made visible by dyeing the ice cube with food coloring and by adding buoyant paper pellets on the free surface. The motion of the dyed vortex was also observed from the side of the tank. The velocities were measured by tracking the paper pellets on the surface. A computer system with a frame-grabber card and the image processing software DigImage (Dalziel, 1992) was used to acquire and process the images from the videos of the flow. Typically, fewer than 500 paper pellets were located in each frame and the velocities were obtained by sampling the video at a frequency of approximately 2 Hz. Automatic matching of these locations to the ones in previous frames produced the tracking files. Particle velocities were calculated over five samples and the velocity field was obtained by mapping the individual velocity vectors onto a rectangular grid using a spatial averaging over 0.04 m and time averaging over 1.3 s. The vorticity was calculated from this gridded velocity data. The error in the velocities is estimated to be somewhat larger than 5% (Linden *et al.,* 1995), whereas the error in the derived fields is estimated to be approximately 10%.

a. Laboratory model approximations

In the laboratory model described above, two major simplifications have been made:

i. Meddy modeled as a barotropic vortex. The idealized laboratory experiments presented in this paper consider a vortex which extends for almost the whole fluid depth and is embedded in a homogeneous fluid, while meddies are interior features and move within a stratified environment. However, the signature of a meddy, as shown by density sections,

extends all the way to the ocean surface down to at least 2000 m depth (Richardson *et al.,* 2000) showing that the vortex dynamical structure extends beyond the layers occupied by temperature and salinity anomalies. Hence, with these experiments, we attempt to address only the dynamics of such "barotropic" meddy structure, extending from the surface down to 2000 m, interacting with an island or seamount. We are neglecting the effects of a stratified environment that are possibly important in determining the stability of the meddies and the advection mechanism. The present paper focuses on stable vortices and does not address the otherwise interesting problem of an unstable vortex interacting with obstacles. Furthermore, we consider only self-advected vortices and do not focus on the influence of the advection mechanism on the interaction. Considering a barotropic vortex is possibly the weakest point of the model, but the simplicity of the homogeneous versus the stratified experiments made it more appropriate for this idealized study. The above considerations, together with the good agreement between the results obtained using a similar model (C02) and the oceanic observations, led us to believe that stratification does not invalidate the relevance of the results discussed herein.

ii. Meddy modeled as a cyclonic vortex. Although meddies are anticyclonic vortices, in the laboratory we could not reproduce barotropic anticyclones since they tend to be centrifugally unstable (Kloosterziel and van Heijst, 1991) and become non-axisymmetric in a few rotation periods. As shown by C02, the use of cyclonic vortices does not limit the generality of the results, which can be easily extended to anticyclones. In particular, the circulation equation around the obstacle and the equation relating the streamer velocity to the vortex velocity (see Eq. (10)) still holds for anticyclones. The streamer, instead of moving counterclockwise, will go clockwise around the obstacle since the vortex velocity for an anticyclone is negative. Hence, the streamer formation and motion around the obstacle is believed to apply to an anticyclone in the same way it has been shown to apply to a cyclone. Furthermore, the condition for bifurcation to occur, $400 \leq Re \leq 1100$, only takes into account the velocity of the streamer (see Eq. (1)). Hence, provided the streamer forms for an anticyclone interacting with an obstacle, and moves around the obstacle in a clockwise direction, the hypothesized condition for vortex bifurcation should still hold. We believe that the two mechanisms described above should apply to anticyclones in a similar manner as they do to cyclones. The differences between cyclones and anticyclones in terms of their propagation direction, stability properties, etc., are not investigated in the present paper and the hypothesized mechanism for bifurcation does not rely on any dynamics that is different (a part from the sign) between the two opposite sign vortices.

3. "Glancing" interactions

Previous experimental results by C02 have shown that bifurcation of a cyclonic self-propagating vortex colliding with a right circular cylinder occurs provided $0.2 \leq D/d \leq 1$ and $Y/R \leq 0$. Furthermore, for $Y/R \leq 0$ the value of Re for bifurcation to occur has been experimentally found to be $400 \leq Re \leq 1100$, as shown in Figure 12 of C02.

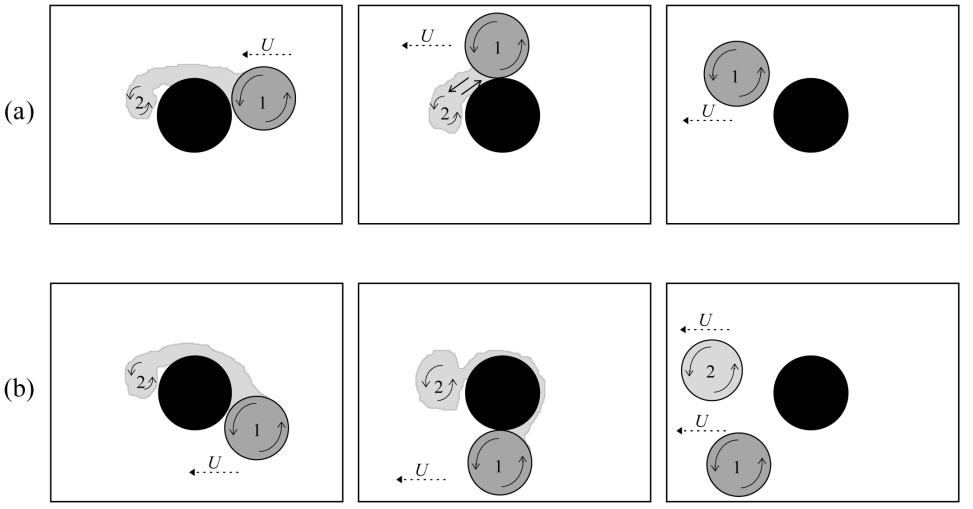

Figure 3. Sketch illustrating a self-propagating cyclonic vortex interacting with a cylinder. The vortex self propagated at a velocity U indicated by the dashed arrow. (a) $Y/R < 0$, North hit. (b) $Y/R \geq 0$, South and Central hit. (1) indicates the original vortex and (2) the newly-formed vortex. (From Fig. 5 in C02.)

The physical explanation given by C02 for bifurcation occurring only for southern or central interaction ($Y/R \leq 0$) is as follows: for values $Y/R > 0$ (northern interaction), the streamer started forming a new cyclonic vortex in the wake of the cylinder. However, the original vortex passed around the northern side of the cylinder, overtook and merged with the newly-formed vortex and continued its westward drift as a single coherent structure as shown in Figure 3a. A different scenario occurred for $Y/R \leq 0$. As before, the streamer formed a new cyclonic vortex in the wake of the cylinder but the original vortex passed around the southern side of the cylinder, did not overtake the newly-formed vortex and continued its westward drift independent of the new vortex. Meanwhile the new vortex completed its formation and began drifting westward independent of the original vortex (see Fig. 3b). Furthermore, for values of $Re < 400$, corresponding to $D/d > 1$, the streamer velocity is too small and, therefore, the streamer goes around the cylinder as a potential flow without forming a vortex in the wake. For values of $Re > 1100$, corresponding to $D/d < 0.2$, the streamer velocity is too large and the vortex moved undisturbed past the cylinder without major changes.

However, for values of $Y = Y_k \equiv -(r + R)$, the vortex will just "kiss" the southern part of the obstacle, hence for $Y/R < Y_k/R$ the vortex will not interact with the obstacle. Furthermore, for values of $Y_k/R \leq Y/R \leq 0$ (Fig. 4), bifurcation will only occur if the streamer, peeling off the outer edge of the vortex, goes counterclockwise around the obstacle with an average velocity v_s above a critical value, i.e.,

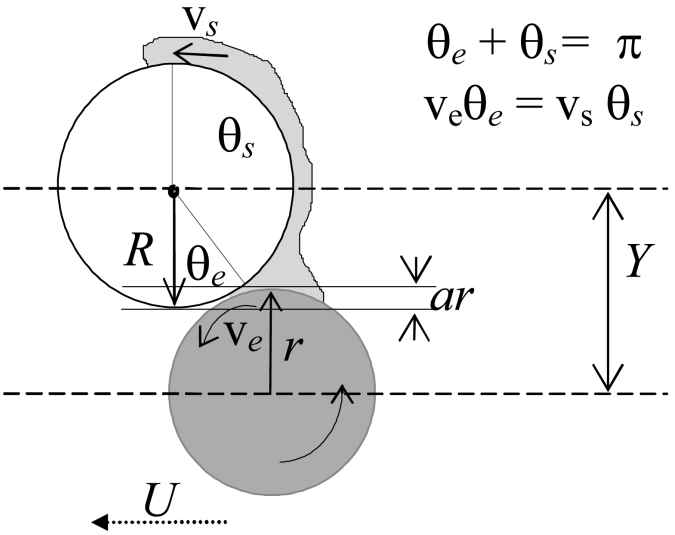

Figure 4. Sketch illustrating a glancing interaction (not to scale) and the relevant parameters defined in Section 3. The top right equations indicate the assumption made that $\theta_e + \theta_s = \pi$ and the relationship between the streamer velocity, v_s, and the velocity of the vortex fluid along the cylinder, v_e, found by C02.

$$Re = \frac{v_s L_{\max}}{\nu} \geq 400, \tag{1}$$

where $L_{\max} = \max[D, d]$ and $\nu = 10^{-6}\,\mathrm{m^2\,s^{-1}}$ is the kinematic viscosity. Figure 4 illustrates a glancing interaction for which the streamer undergoes a distance $S_s = R\theta_s$ with an average velocity v_s, and the vortex interacts with the cylinder over a distance $S_e = R\theta_e$, along which the velocity of the vortex fluid is v_e. Recalling the results from C02, obtained using a circulation integral argument, and assuming $\theta_e + \theta_s = \pi$, the streamer velocity can be expressed as

$$v_s = \frac{v_e(\pi - \theta_s)}{\theta_s}. \tag{2}$$

In particular, v_e is the velocity of the vortex fluid along the cylinder outer wall and, in the laboratory, it is measured during the initial stage of the interaction. Furthermore, v_s is the streamer velocity, assumed to be constant within and along the obstacle boundary layer, and it is measured along the northern part of the obstacle, just before the streamer leaves the obstacle. For $L_{\max} = d$, i.e. $D/d \leq 1$, and substituting Eq. (2) in Eq. (1), one can see that bifurcation will happen only if the streamer undergoes a distance $S_{scrt} = R\theta_{scrt}$ where

$$\theta_{scrit} = \frac{2r\pi v_e}{2rv_e + 400\nu}. \tag{3}$$

We then define that a vortex is "glancing" an obstacle when

$$\frac{Y}{R} = -1 - (1 - a)\frac{d}{D}, \tag{4}$$

where a is the fraction of the vortex radius that interacts with the obstacle (Fig. 4), bounded between $0 \leq a \leq R/r$. Geometrically, and from Eq. (3), we can determine the value of a above which the critical condition for bifurcation is satisfied

$$a_{crit} = D/d\left[1 - \sin\left(\frac{\pi}{2} - \frac{400\nu\pi}{2rv_e + 400\nu}\right)\right]. \tag{5}$$

Substituting Eq. (5) in Eq. (4) gives an expression of Y/R below which bifurcation is not expected, although the conditions $0.2 \leq D/d \leq 1$ and $Y/R \leq 0$ are satisfied. For those values of Y/R, the vortex is glancing the obstacle and the interaction is "weak" in the sense that the streamer going around the obstacle in the counterclockwise direction leaves the obstacle with a velocity too small for $Re \geq 400$ to be satisfied and form a new vortex in the wake. The value of a_{crit} depends not only on the ratio D/d, but also on the value of the radius of the vortex alone and the velocity of the vortex fluid along the cylinder, v_e. We will verify the accuracy of Eqs. (5) and (4) in Sections 5 and 6 where we will consider the velocity of the vortex fluid along the cylinder constant and equal to $v_e = 0.005$ m s^{-1} and only two values of $r = 0.035$ m and $r = 0.055$ m, since those values are the most representative for the experiments discussed in these sections.

This new prediction of the fate of a glancing interaction uses the criteria for bifurcation, $Re \geq 400$, and the relation between the streamer and the vortex velocities, $v_s\theta_s = v_e\theta_e$, found by C02. However, its novelty lies in applying these known criteria to determine when bifurcation occurs for collisions in which the whole vortex does not interact with the obstacle, but rather with just a peripheral part. This new distinction in the interaction process (i.e. "glancing interactions") and the identification of a_{crit}, is fundamental in determining the dynamical reason why some of the vortices interacting with an obstacle did not bifurcate, although $Y/R \leq 0$ and $0.2 \leq D/d \leq 1$. Eqs. (5) and (4), represented by the solid and dashed-dotted lines in Figures 9 and 13, clearly demarcate the lower boundary of the bifurcation region missing from the analysis of C02. Experiments in C02 did not investigate values of Y/R for which the above critical condition was not satisfied.

4. Influence of horizontal cross sectional geometry

a. Circulation around an ellipse

The circulation around an elliptical cylinder for a single layer of homogeneous fluid can be derived following the discussion in C02 that investigated a circular cylinder. The difference from the circular cylinder lies in the arc element of an ellipse, S_{ell} shown in Figure 5, being different from that of a circle, $S_{cir} = R\theta$. Integrating the tangential component of the momentum equation around a closed circuit C around the obstacle

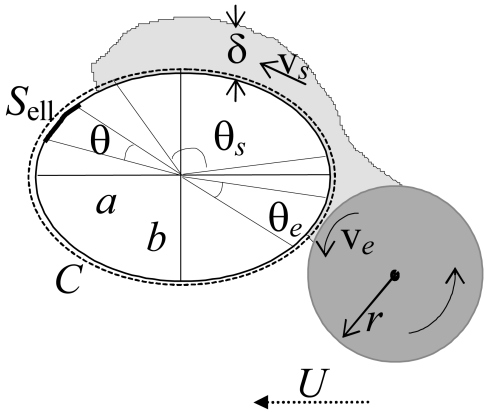

Figure 5. Sketch illustrating the interaction of a vortex with an elliptical cylinder (not to scale). After the self-propagating cyclonic vortex came in contact with the elliptical cylinder, fluid peeled off the outer edge of the vortex and a streamer went around the cylinder in a counterclockwise direction, with a velocity v_s. S_{ell} represents the arc element of an ellipse.

(Godfrey, 1989; Pedlosky *et al.,* 1997), we obtained an equation for the circulation around C. Since the velocity normal to the obstacle is zero, assuming the dissipation of horizontal momentum to be due solely to lateral friction and to be equal to $\nu\nabla^2\mathbf{u}$, and in the case of no-slip boundary condition, i.e. the velocity $\mathbf{u}$ is identically equal to zero on the boundary C, the circulation equation reduces to Eq. (4) in C02

$$\oint_C \nu\nabla^2\mathbf{u} \cdot \mathbf{t}ds \simeq \oint_C \nu \frac{v}{\delta^2} ds = 0, \tag{6}$$

where we scaled the horizontal thickness of the streamer with the boundary layer thickness δ and the tangential component of the velocity $\mathbf{u}$ within the boundary layer with a characteristic velocity v. The value of an arc element of an ellipse S_{ell} is given by

$$S_{ell} = b \int_0^{\gamma} \sqrt{1 - k^2 \sin^2 \gamma'}\, d\gamma = bE(\gamma, k), \tag{7}$$

where b is the ellipse's semi-axis in the y direction and $E(\gamma, k)$ is an incomplete elliptic integral of the second kind with elliptic modulus

$$k = \sqrt{1 - \frac{a^2}{b^2}}, \tag{8}$$

with a being the ellipse's semi-axis in the x direction. The relationship that links the angle θ, determining the ellipse's arc (Fig. 5), and the parameter γ is

$$\theta = \tan^{-1}\left(\frac{b}{a}\tan\gamma\right). \tag{9}$$

Given the approximations made to obtain Eq. (6), the use of the incomplete elliptic integral to make the estimates below is not necessary. However, we preferred the use of Eq. (7) to give a compact expression of an arc element of an ellipse explicitly indicating its dependence on both the major and minor axis and the angle θ span by the arc element.

Hence, considering that δ, ν and b are constants, Eq. (6) becomes

$$\oint_C v\,ds = v_s E(\gamma_s, k) - v_e E(\gamma_e, k) = 0, \tag{10}$$

where v_s and v_e have the same meaning as in Section 3 and γ_s and γ_e are obtained by Eq. (9) using the angles θ_s and θ_e, respectively, shown in Figure 5. Eq. (10) corresponds to Eq. (6) in C02, but for an elliptical obstacle, and its validity has been confirmed experimentally as discussed in Section 4c.

This new expression brings to light the importance of the path's length that the streamer undergoes. For the geometry investigated by C02 and constant v_e and θ_e, the angle θ_s was the parameter determining the magnitude of the streamer velocity, v_s, and consequently of the Reynolds number. This new derivation of Eq. (10) illustrates that the relevant parameter determining the streamer velocity once it leaves the obstacle is not the angle the streamer spans, θ_s, but the length of the path it undergoes, $bE(\gamma_s, k)$, which, for a fixed angle θ_s, is a function of both the ellipse's semi-axes, a and b. This new finding is fundamental in explaining, in the next section, why the relevant parameter for bifurcation to occur is the equivalent diameter, given by a combination of a and b, and not any of the elliptical dimensions separately.

b. Experimental results

The qualitative behavior of a vortex interacting with an elliptical cylinder is similar to that described in C02. After the self-propagating cyclonic vortex came in contact with the obstacle, fluid peeled off the outer edge of the vortex and a streamer went around the cylinder in a counterclockwise direction (see Fig. 5). Under the right conditions, this fluid formed a new cyclonic vortex in the wake of the cylinder while the original vortex passed around the obstacle. Hence, the original vortex bifurcated into two vortices, one containing the original core and the other containing the fluid of the streamer. However, if the same parameters Y/R and D/d as in C02 are considered, where in this case $D = 2R$ is the axis of the ellipse orthogonal to the direction of propagation of the vortex (see Fig. 2), bifurcation is still observed to occur for $Y/R \leq 0$, but no longer observed for $0.2 \leq D/d \leq 1.0$. Hence, the parameter D/d does not collapse the data and does not seem to be a relevant parameter for a vortex interacting with an elliptical cylinder.

c. Discussion

The above-mentioned disagreement between the present results and the results of C02 is not surprising when one considers that a new cyclonic vortex in the wake of a cylinder is expected to form when the fluid in the streamer passes the obstacle with a high enough Reynolds number ($400 \leq Re \leq 1100$), as found by C02. From Eq. (10), it is clear that the average streamer velocity around the obstacle, v_s, depends on the magnitude of the elliptical arc the streamer undergoes, $bE(\gamma_s, k)$, the larger the arc, the smaller the streamer velocity v_s for a given velocity of the vortex fluid along the cylinder v_e and angle θ_e. It is then expected that the relevant parameter which influences the bifurcations is the path that the streamer follows, and not the dimension of the obstacle orthogonal to the motion of the vortex. In the case of a circular cylinder, the path that the streamer follows depends on the diameter D of the cylinder. However, in the case of an elliptical cylinder the path the streamer follows does not depend on any of the elliptical dimensions separately, but on the combination of the two. Hence, it is observed that the length (D) of the elliptic axis orthogonal to the direction of propagation of the vortex does not influence the bifurcation phenomenon, but rather the relevant lengthscale is the equivalent diameter of the ellipse,

$$D_{eq} = \sqrt{2(a^2 + b^2)}, \tag{11}$$

defined as the diameter of the circumference having the same perimeter as the ellipse.

The regime diagram of the experimental runs with a cylindrical obstacle having an elliptical cross section is shown in Figure 6. Bifurcation was only observed for central and southern interactions, i.e. $Y/R \leq 0$, in agreement with C02. A second condition that needs to be satisfied for bifurcation to occur is $D_{eq}/d \leq 1$ corresponding to $Re \geq 400$. The minimum value of D_{eq}/d for which bifurcation occurs was not investigated since only two ellipses were used. These ellipses were designed to have the minor m and major M axis such that a vortex of a specific diameter d' would bifurcate, $0.2 \leq m/d' \leq 1$, and would not bifurcate, $M/d' > 1$, when the minor/major axis was located orthogonally to the direction of propagation of the vortex. The equivalent diameter of the ellipse was such that $0.2 \leq D_{eq}/d' \leq 1$ for the first ellipse and $D_{eq}/d' > 1$ for the second. Bifurcation of a vortex with diameter d' was only observed when using the first ellipse regardless of its orientation to the direction of propagation of the vortex. This confirms the above argument that the relevant parameter which influences the bifurcations is the path that the streamer follows, i.e. D_{eq}, and not the dimension of the obstacle orthogonal to the motion of the vortex, i.e. neither m nor M.

In Figure 7, both (a) the velocity and vorticity field and (b) the surface particle paths show the presence of a new cyclonic vortex downstream of the elliptical cylinder, while the original vortex is moving around the southern part of the obstacle. From the velocity fields, we measured the velocity of the streamer before it detached from the obstacle, and the maximum azimuthal velocity of the vortex, where it interacted with the obstacle, in order to verify that Eq. (10) was satisfied. The good agreement shown in Figure 8 suggests that, as predicted by Eq. (10), the dissipation due to the fluid within the vortex moving along the

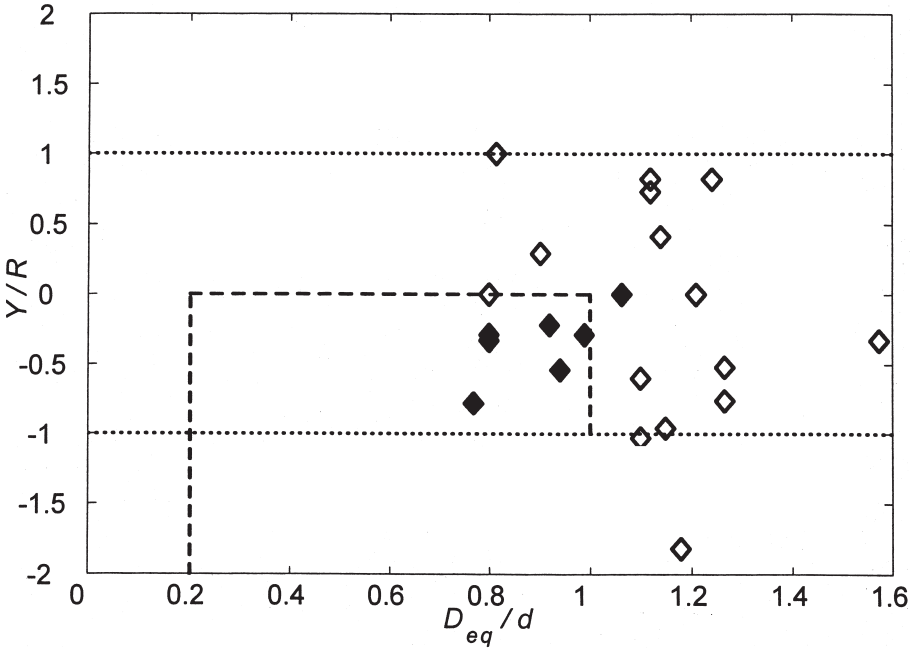

Figure 6. Regime diagram for a self-propagating vortex colliding with an obstacle having an elliptical cross section. The dashed line bounds the region where bifurcation was observed by C02. The dotted lines indicate the northern ($Y/R = 1$) and southern ($Y/R = -1$) sides of the obstacle. Full (open) symbols represent experiments for which bifurcation was (was not) observed.

obstacle in a clockwise direction (not to be confused with the velocity within the vortex that keeps being counterclockwise) over an arc of ellipse S_e, was balanced by the dissipation due to the fluid within the streamer going around the obstacle in the opposite direction (counterclockwise) over an arc of ellipse S_s.

5. Influence of the obstacle height

a. Experimental results

The second set of experiments investigated the influence of the obstacle height, h, on the bifurcation mechanism. We utilized a circular right vertical cylinder as in C02 in order to compare our results with the case in which the obstacle occupied the whole water depth. Bifurcation of a self-propagating vortex was observed for the same values of the parameters D/d and Y/R as in C02, provided $h/h_0 \geq 0.85$ (Fig. 9). The qualitative behavior was similar to the one described in the previous section and the velocity and vorticity fields for an experiment in which $h/h_0 = 0.85$ and the original vortex moves around the northern part of the obstacle are shown in Figure 10. In this experiment, two new vortices formed after the collision of the original vortex with the obstacle. The

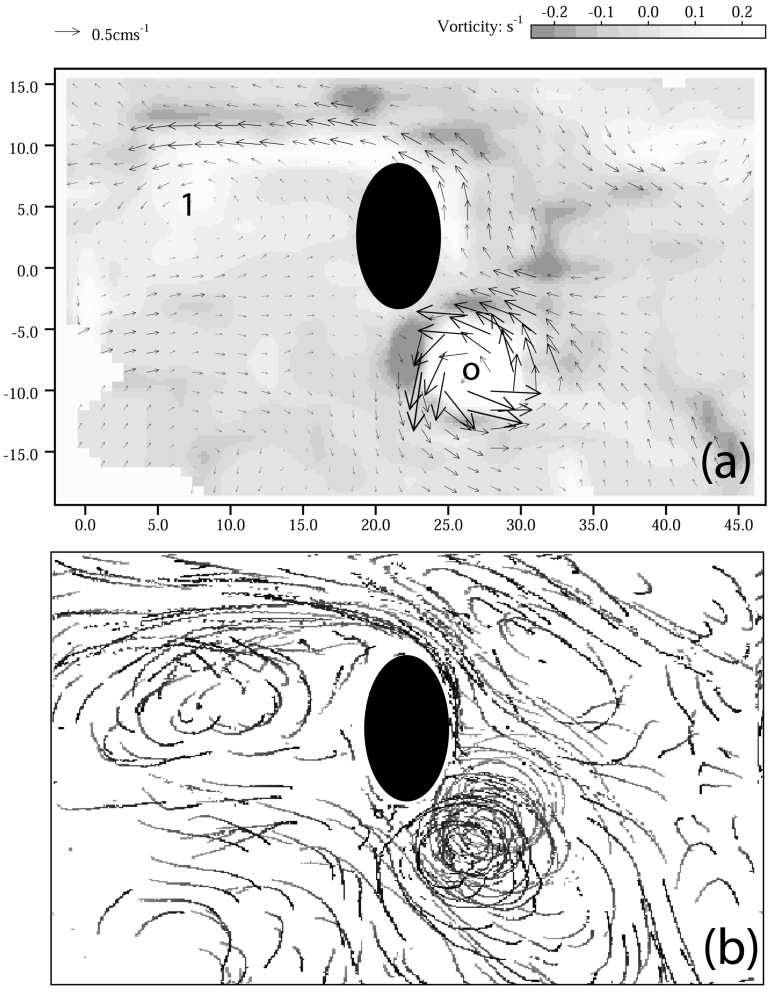

Figure 7. (a) Velocity and vorticity field of a vortex interacting with an elliptical cylinder for $D_{eq}/d = 0.80$ and $Y/R = -0.29$. (b) Buoyant surface particle trajectories for a 30-second time interval centered at the instant the velocity field was calculated. Gray (black) trajectories indicate earlier (later) times. The two figures cover the same planar field of view and the labels of (a) indicate distances in cm. Labels o and 1 indicate the original vortex and the new vortex, respectively.

differences observed when comparing the results to the experiments having a cylinder height equal to the total water depth, are that the self-propagating vortex, after the streamer went around the cylinder and formed one or more new vortices, was observed to move around the "northern" part of the obstacle after a "southern" collision provided $-0.53 \leq Y/R \leq 0$. However, for $-1.00 \leq Y/R < -0.53$ the original vortex moved around the southern part of the obstacle as in C02. Furthermore, for $h/h_0 = 0.85$ and $Y/R < -1$

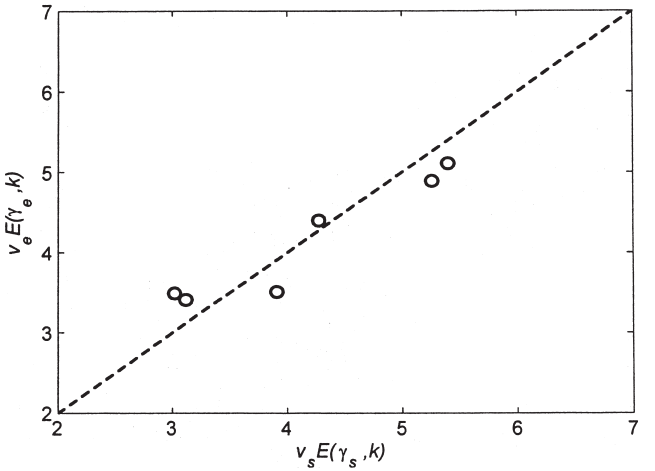

Figure 8. Absolute value of the terms in Eq. (10). The subscript *s* indicates the fluid within the streamer, the subscript *e* indicates the fluid within the vortex. The dashed line represents unity.

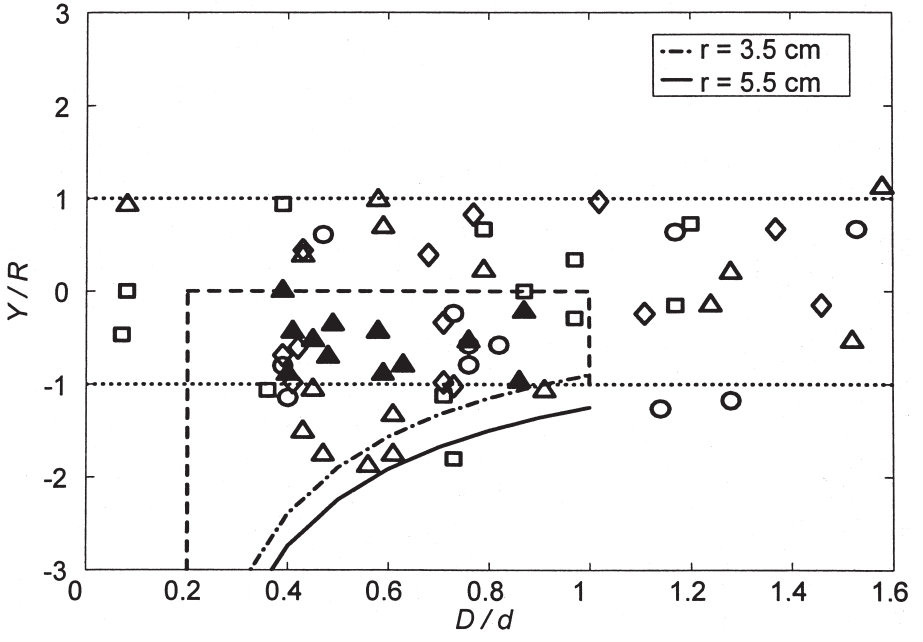

Figure 9. Regime diagram for a self-propagating vortex colliding with a circular cylinder of depth $h/h_0 = 0.25$ (□), $h/h_0 = 0.50$ (◇), $h/h_0 = 0.75$ (○) and $h/h_0 = 0.85$ (△). Full (open) symbols represent experiments for which bifurcation was (was not) observed. The dashed and dotted lines are the same as in Figure 6.

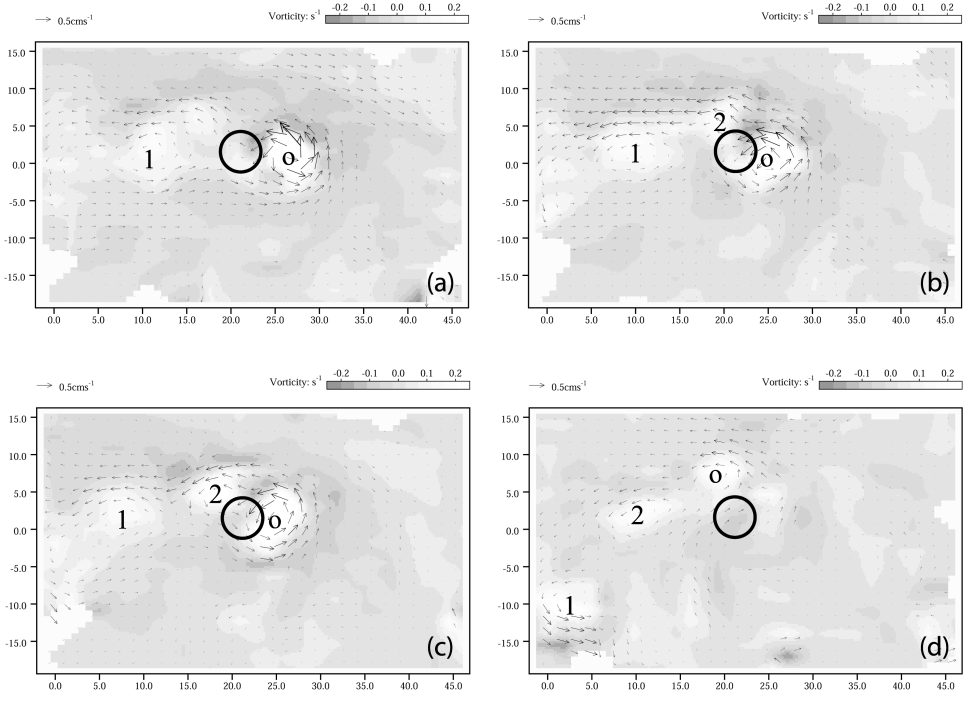

Figure 10. Velocity and vorticity fields of a vortex interaction with a circular cylinder for $h/h_0 = 0.85$, $D/d = 0.44$ and $Y/R = -0.53$. (a) 66 s, a new vortex (1) formed in the wake of the cylinder; (b) 76 s, a second vortex (2) is forming in the wake of the cylinder; (c) 88 s, the second vortex formed and the original vortex (o) started moving around the obstacle; (d) 164 s, the original vortex (o) moved around the "northern" side of the cylinder and the first vortex (1) encountered the left sidewall of the tank and is moving south along it. The solid circle indicates the position of the obstacle.

bifurcation was not observed. In Figure 9 the curves representing Eq. (4) are plotted for values of a_{crit} corresponding to $r = 0.035$ m and $r = 0.055$ m. Most of the experiments for which bifurcation does not occur (open triangles), although $0.2 \leq D/d \leq 1$ and $Y/R \leq 0$, lie close or within these two curves indicating that these vortices are "glancing" the obstacle and the critical condition for bifurcation to occur is not satisfied, as explained in Section 3.

For values of $h/h_0 = 0.75$ and $Y/R < 0$, we observed that after the vortex approached the obstacle, part of the vortex moved over the obstacle as shown by the surface particle trajectories in Figure 11. Once over the obstacle, the particle trajectories turned sharply northward and, after the fluid moved off the obstacle, turned sharply westward and kept moving westward following isobaths. Hence, for values of $h/h_0 = 0.75$, the collision of the vortex with a submerged cylinder resulted in the fluid within the outer edge of the vortex to separate, move over the obstacle, and continue its westward motion on a different isobath than the vortex. The behavior described above was observed only for values of

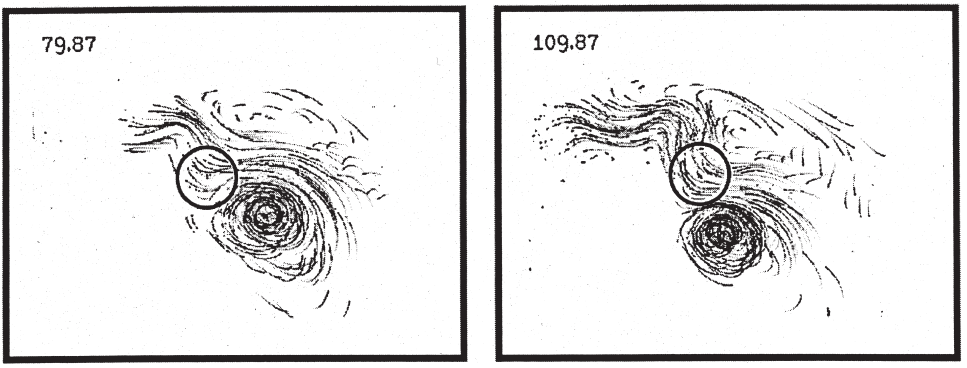

Figure 11. Buoyant surface particle trajectories for a 30-second time interval ending at the time (in seconds) indicated on the top left of each figure. $h/h_0 = 0.75$, $D/d = 0.82$ and $Y/R = -0.59$. The solid circle indicates the position of the obstacle.

$h/h_0 = 0.75$ and $Y/R < 0$, while for values $Y/R \geq 0$, the vortex was observed to move around the northern side of the obstacle without any deformation of the particle trajectories.

For values of $h/h_0 = 0.50$, the vortex moved around the obstacle, either around the "northern" side for values $Y/R > 0$ or the "southern" side for values of $Y/R \leq -0.3$. For $-0.3 < Y/R \leq 0$, the whole vortex moved over the obstacle and the trajectory of the center of the vortex was deflected northwestward until the vortex moved off of the obstacle on the northwestward part of it. Once off the obstacle, the vortex moved westward following isobaths.

Finally, for values of $h/h_0 = 0.25$ and $-0.3 < Y/R \leq 0$, the vortex moved over the obstacle and a modification of the center of the vortex trajectory was observed, as described above for the case $h/h_0 = 0.50$. However, for $h/h_0 = 0.25$, the northwestward movement of the whole vortex was less pronounced.

b. Discussion

The results obtained with $h/h_0 = 0.75$ illustrated in Figure 11 can be explained as follows: the depth of the water column located on the outer edge of the vortex and moving over the obstacle is decreased from a depth h_0 to a depth $h_0 - h$, where h_0 is the vortex depth and h is the obstacle depth. In order to conserve potential vorticity, the water column must acquire a vorticity ζ given by

$$\frac{f}{h_0} = \frac{f + \zeta}{h_0 - h}. \tag{12}$$

Hence $\zeta = -fh/h_0$ and the water column above the obstacle acquires anticyclonic vorticity. This is confirmed in Figure 11 by the particle trajectories that move over the obstacle and are deflected toward the northern side of the tank. Once the water column has

moved off the obstacle, it is stretched to approximately its original depth h_0 and, in order to conserve potential vorticity, it stops spinning anticyclonically. Then, it continues moving westward due to the bottom slope as shown in Figure 11. The particle paths, after moving northward, turn sharply westward and move following an approximately constant isobath. The final result of this interaction is the deformation of the trajectory of the fluid within the outer edge of the vortex. The formation of a "wake" can be observed indicating that this fluid first experiences an anticyclonic motion; second, it experiences a cyclonic motion and finally moves westward.

The behavior described above, observed for $h/h_0 = 0.75$, is consistent with previous laboratory experiments investigating the effect of nonlinear processes, i.e. Rossby number, on Taylor-Proudman column formation (Hide and Ibbetson, 1966). For a uniform flow past a submerged cylinder, as the Rossby number increases, the fluid starts penetrating the region above the cylinder. As the Rossby number increases further, nonlinear effects produce a strong cross-flow over the obstacle. The behavior of a uniform flow past an obstacle for small Rossby number on an *f*- or β-plane, with inclusion of viscosity and/or inertial effects, has been extensively studied in the past (see McCartney (1975) for a summary on these studies). However, in the present work the value of the Rossby number is $R_o = \zeta/f \approx 0.6 - 1$ and the good agreement with Hide and Ibbetson (1966) experiments is expected. A more recent study of a narrow current impinging upon a seamount by Zhang *et al.* (1994) also illustrates the presence of anticyclonic vorticity atop the obstacle and regions of cyclonic vorticity on the right leeside of the obstacle, again in agreement with Figure 11.

For values of $h/h_0 = 0.50$, the behavior observed for $-0.3 < Y/R \leq 0$ suggests that the outer edge of the vortex is not affected by the "squeezing" and "stretching" of the water columns when moving over the obstacle, possibly because the relative vorticity generated to conserve potential vorticity (see Eq. (12)) is not large enough to overcome the particles' velocity and modify their trajectories. This result is consistent with the scenario described above, since the relative vorticity production due to conservation of potential vorticity is proportional to h/h_0. However, when the whole vortex moves over the obstacle, it then follows contours of constant potential vorticity (i.e. constant depth) during its westward motion; hence, its center moves towards the northern part of the obstacle.

6. Influence of sloping sidewalls

a. Experimental results

The influence of having an obstacle with sloping walls instead of vertical walls was investigated using a truncated cone extending throughout the entire fluid column depth. Only two relatively steep slopes were used, $s' = 83°$ and $s' = 70°$, and the motivation of this choice is given in the next section. The qualitative behavior of a self-propagating vortex interacting with the conic obstacle and bifurcating into two vortices was similar

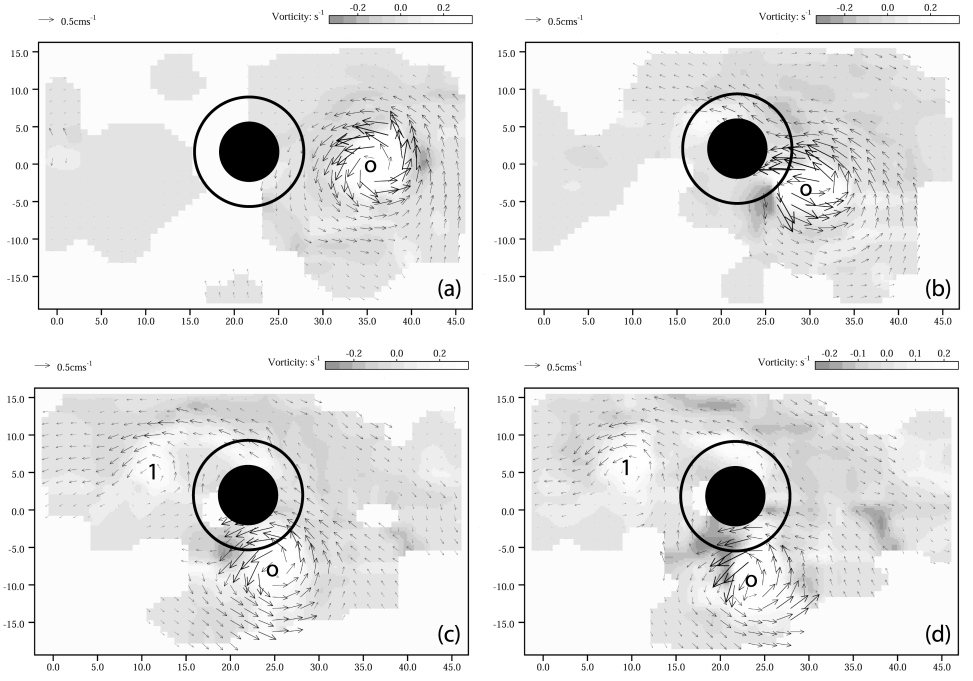

Figure 12. Velocity and vorticity fields of a vortex interacting with an obstacle with sloping walls ($s' = 70°$). (a) 16 s, (b) 50 s; (c) 84 s; (d) 92 s. $D_{av}/d = 0.91$ and $Y/R_{av} = -0.47$. Labels o and 1 indicate the original vortex and the new vortex, respectively. Full (open) circle indicates the position of the top (bottom) part of the cone.

to the cases described in the previous sections (see Fig. 12). No differences were observed between experiments using cones with different sidewall slopes and the results obtained by C02 with a vertical wall. For both slopes the vortex was observed to bifurcate for $0.16 \leq D_{av}/d \leq 1.0$ and $Y/R_{av} \leq 0$, where $R_{av} = D_{av}/2$, as shown in Figure 13. If we were to use either the top or base values of the diameter in the ratio D_{av}/d, instead of the geometric average of the two, the experimental data showing bifurcation would not collapse into the region shown in the regime diagram. Finally, for some experiments the vortex did not bifurcate, although $0.2 \leq D_{av}/d \leq 1$ and $Y/R_{av} \leq 0$. As shown in Figure 13, these experiments lie within the curves representing Eq. (4) for values of a_{crit} corresponding to $r = 0.035$ m and $r = 0.055$ m, indicating that these vortices are "glancing" the obstacle and the critical condition for bifurcation is not met, as explained in Section 3.

b. Discussion

The results obtained using an obstacle with sloping sidewalls indicate that the bifurcation mechanism, provided the slopes are steep, is similar to the one observed when using

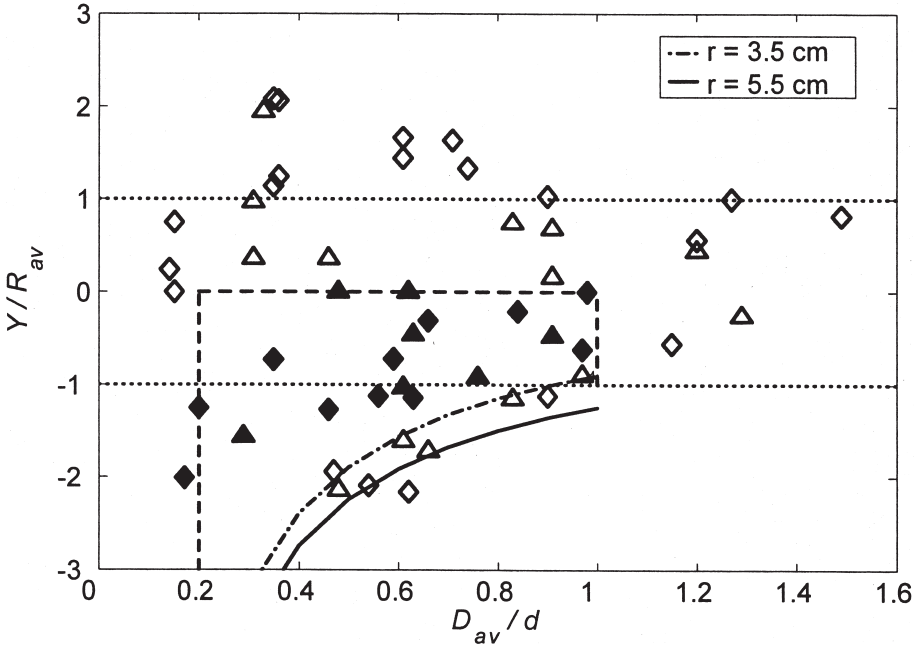

Figure 13. Regime diagram for a self-propagating vortex colliding with an obstacle having sloping sidewalls and a circular cross section. The dashed and dotted lines are the same as in Figure 6. Full (open) symbols represent experiments for which bifurcation was (was not) observed. ◇ indicates a slope of 83° and △ indicates a slope of 70°.

vertical sidewalls (C02). In order to reproduce in the laboratory the dynamics introduced by the sloping sidewalls of a seamount, we assumed that the ratio of the relative vorticity of the vortex $\zeta = (U/R)$, where U and R are characteristic velocity and length scales, and relative vorticity induced by the sloping topography $\zeta_{topo} = -(fs'R/h_0)$ (see Section 5b and Eq. (12) in which, for a sloping topography, $h = s'R$) is the same both in the laboratory experiments and in the ocean, namely

$$\frac{U_{lab}}{\left(\frac{s'f}{h_0}\right)_{lab} R_{lab}^2} = \frac{U_{oce}}{\left(\frac{s'f}{h_0}\right)_{oce} R_{oce}^2}. \tag{13}$$

Meddies have been observed to drift at a velocity of ~0.05 m s^{-1} and have a diameter of approximately 10^5 m. The sloping walls of a seamount are typically $s'_{oce} \approx 0.04$, while $f \approx 10^{-4}$ s^{-1} and $h_0 \approx 1000$ m. In the laboratory, $U_{lab} \approx 0.002$ m s^{-1}, $R_{lab} \approx 0.05$ m, $f = 0.25$ s^{-1} and $h_0 = 0.10$ m. Hence, Eq. (13) gives a value of the slope $s'_{lab} = 64$ equivalent to $\theta_{lab} = 89.1°$. This simple scaling analysis was the justification for C02 to use vertical walls. In the present study, we investigated the influence of the obstacle's sidewalls still steep in the laboratory, 83° and 70°, and equivalent to values in the ocean,

$s'_{oce} = 5.0\ 10^{-3}$ and $s'_{oce} = 1.7\ 10^{-3}$, respectively. These oceanic values are smaller than shelf break slopes in the Middle Atlantic Bight, but of the same order of magnitude than the slope of the continental shelf on the west coast of the United States. Hence, our results indicate that, even if the oceanic seamounts would present much gentler sloping walls, the bifurcation mechanism would not be modified when compared to steep sidewall seamounts. Note that the obstacle slope used in the present experiments is an order of magnitude larger than the one used by Carnevale *et al.* (1991) ($\theta \approx 6°$) to investigate the behavior of a barotropic vortex over a broad topography.

Finally, the truncated cones were designed to have the base diameter, D_b, and the top diameter, D_t, such that a vortex of a specific diameter d' would not bifurcate neither for the base diameter, i.e. $D_b/d' > 1$, nor for the top diameter, i.e. $D_t/d' < 0.2$. However, the vortex with a diameter d' did bifurcate. Hence, the experimental results suggest that neither D_b nor D_t is the correct lengthscale to collapse the data. Figure 13 shows that the average diameter D_{av} is the lengthscale determining when bifurcation occurs, confirming that the flow within the vortex is barotropic and two-dimensional.

7. Comparisons with observations

A recent review paper by Richardson *et al.* (2000) summarizes the results of three experiments: Semaphore, Iberian Basin and AMUSE that overlapped during 1993–1994 and resulted in the tracking of 21 meddies by means of floats. Some of the meddies have been observed to interact with seamounts which either disturbed or disrupted the trajectory and swirl velocity of the vortex. Bifurcation of the original vortex into two vortices was observed only in one case (Meddy 26). The scarcity of observations of vortex bifurcation could be explained by the difficulty of the method used, since the presence of at least two floats in the vortex is necessary. The above mentioned observation compared favorably to previous laboratory experiments by C02.

We note that, in order to compare the results obtained with a cyclonic vortex to anticyclonic vortices, the theoretical approach in Section 4a can be extended as discussed in Section 2a(ii). One then finds out that the streamer of fluid peeling off the outer edge of an anticyclonic vortex will go around the obstacle in a clockwise direction, i.e. around the southern side of the obstacle. Consequently, an anticyclonic vortex interacting with an obstacle will bifurcate for $Y/R \geq 0$. As mentioned in Section 5b, in the present experiments the value of the Rossby number was approximately constant $R_o \approx 0.6 - 1$ and much larger than the approximate value 0.04 pertinent to meddies. We will then compare the values of the nondimensional parameters, D/d, Y/R and h/h_0 varied in the present experiments with those observed in the ocean and leave to the next section a discussion on the possible role of the Rossby number on the bifurcation mechanism. It should be noticed that the present experiments were designed to have values of the nondimensional gradient of background vorticity due to the obstacle side walls $\beta_* = \beta R^2/U$ identical to the ocean values, as discussed in detail in Section 6b. Finally, the sloping bottom ($s = 0.5$), inducing the vortex westward drift, gives value of $\beta_{*lab} = 1.56$

Table 2. Relevant dimensional and nondimensional parameters for collision of Meddy 13 with the first four seamounts and Meddy 24 with the last seamount. E = elliptical; C = conical.

Seamount	Geometry	Depth of peak (m)	h (m)	D_{eq} or D_{av} (10^3 m)	h/h_0	d (10^3 m)	D_{eq}/d or D_{av}/d	Y/R
Josephine	E	200	>1100	31.9	>1	100	0.3	<0
1	C	800	900	10.5	0.8	100	0.1	~0
2	C	1600	100	17.2	0.1	100	0.2	~0
Lion	E	600	1100	26.0	1	100	0.3	<0
Plato	E	476	700	36.3	0.6	120	0.3	<0

in the laboratory, for $\beta = (sf/h_0)$, while the corresponding value in the ocean due to the planetary $\beta_{plan} = 1.57 \times 10^{-11}\ m^{-1}\ s^{-1}$ is approximately half, $\beta_{*oce} = 0.78$. As discussed in Section 2, the value of $s = 0.5$ was chosen to assure that the interaction between the vortex and the obstacle took place before the spindown time.

Meddy 13, with a diameter of approximately $d = 10^5$ m, was observed to collide with several of the Horseshoe Seamounts. First, it went around the southern side of Josephine Seamount, then it moved undisturbed over two un-named seamounts that we will name 1 and 2, and finally it went around the southern side of Lion Seamount (see Fig. 10 of Richardson *et al.,* 2000). The float temperature decreased during these interactions indicating that the vortex water was mixing with ambient water. Two floats were imbedded in the vortex, which both showed similar trajectories. Hereafter, we will consider the meddy centered at 1150 m and extending vertically from 600 m to 1700 m, with a total depth $h_0 = 1100$ m. Josephine Seamount extends beyond the depth of the vortex to 200 m and, at 1000 m depth, it presents an approximately elliptical horizontal cross section. The value of the parameter Y/R is difficult to determine exactly for the following observations but, from the float trajectory, we can estimate if the vortex collision occurred on the southern or northern side of the seamounts. Seamount 1 has a conical geometry between 800 m and 1700 m and interacts with Meddy 13 for a depth $h = 900$ m. Seamount 2 has also a conical geometry between 1600 m and 1700 m and interacts with Meddy 13 for a depth $h = 100$ m. Finally, Lion Seamount presents an elliptical cross section at 1000 m and interaction with Meddy 13 occurs over a depth $h = 1100$ m. The values of the relevant parameters D_{av}/d or D_{eq}/d, Y/R and h/h_0 are shown in Table 2. The present results suggest that Meddy 13, moving around the southern side of Josephine Seamount, would not bifurcate. Then it could move undisturbed over seamounts 1 and 2, since seamount 1, although tall enough, has a diameter too small to cause bifurcation of the meddy, while seamount 2 is too shallow to effect the meddy motion. Hence, the present study suggests that the vortex should not be effected by the presence of seamounts 1 and 2 (see Fig. 9). The parameter values for Lion Seamount are similar to those for Josephine Seamount and Meddy 13, moving around the southern side of the seamount, is not expected to bifurcate. The above predictions, derived using the results discussed in the previous sections, are all in agreement with the observations.

Another interesting comparison with observations can be made when looking at Meddy 24. This large and energetic meddy had a diameter $d = 1.2\ 10^5$ m and passed over a moderately sized seamount, Plato, which has a minimum depth of 476 m (see Fig. 14 of Richardson *et al.,* 2000). Three floats within the vortex showed a slight decrease in temperature during the collision and continued looping for a long time (>1 yr) while their temperature remained constant, indicating that the vortex survived the collision. The Plato Seamount has an elliptical cross section at 1000 m and float MD171 trajectory indicates that the vortex passed on the eastern side of the peak (<476 m) where the depth is approximately 1000 m giving a value for the "interaction" depth $h = 700$ m. The values of the nondimensional parameters in Table 2 suggest that Meddy 24 is expected to move over and around the obstacle as the observations indicate.

8. Conclusions

Laboratory experiments have been performed to investigate the physical processes that govern the bifurcation of a meddy which may occur when it interacts with sea floor topography and in particular the influence of the topography sloping sidewalls, height and cross sectional geometry. The laboratory model is similar to that used in C02 and we compared our results with the findings of this previous work in which the obstacle was extending throughout the entire fluid depth, had right vertical walls, and had a circular cross section. The parameters that regulated the flow in the present experiments were altered when compared to C02. The ratio of the obstacle diameter to the vortex diameter, D/d, as well the parameter measuring the geometry of the encounter, Y/R, have been found to be still relevant to this problem, provided the definition of the obstacle dimension, D, is modified accordingly for the specific obstacle geometry. As in C02, after a cyclonic vortex came in contact with an obstacle, fluid peeled off the outer edge of the vortex and went around the obstacle in a counterclockwise direction. Under the right conditions, this fluid formed a new cyclonic vortex in the wake of the obstacle, while the original vortex passed around it. Hence, the original vortex bifurcated into two vortices provided $Y/R \leq 0$, $0.2 \leq D/d \leq 1.0$ and $h/h_0 \geq 0.85$. In the present study, the dimension, D, of the obstacle is given by the equivalent diameter D_{eq} when the obstacle has an elliptical cross section (Section 4), by the average diameter D_{av}, when the obstacle has sloping sidewalls (Section 6), and by the diameter of the circle when the obstacle is a circular cylinder (Section 5).

When a vortex interacted with a cylinder having a height compared to the whole water column of $h/h_0 = 0.75$ and for values of $Y/R < 0$, we observed that part of the vortex moved over the obstacle. The particle trajectories over the obstacle were modified and, since fluid columns conserve potential vorticity, they turned sharply northward, indicating a gain of anticyclonic relative vorticity. After the fluid moved off the obstacle, the particle trajectories turned sharply westward in a cyclonic manner, and then followed background potential vorticity contours. For values of $h/h_0 < 0.75$, the flow on the outer edge of the vortex was no longer modified. However, for $-0.3 < Y/R \leq 0$, the whole vortex moved over the obstacle; the trajectory of the vortex center was deflected north-westward, while

over the obstacle, and continued its westward motion as soon as the vortex moved off the obstacle.

The behavior of a vortex "glancing" an obstacle has been also investigated using some theoretical arguments (Section 3) whose accuracy has been verified in Sections 5 and 6. Both Figures 9 and 13 show experiments for which bifurcation did not occur although $0.2 \leq D/d \leq 1$ and $Y/R \leq 0$. However, these experiments lie within the curves representing Eq. (4), indicating that these vortices are "glancing" the obstacle and that the critical condition for bifurcation is not satisfied.

In summary the results of this study suggest that bifurcation of a self-propagating cyclonic vortex interacting with an obstacle occurs only when the obstacle height is equal or larger than 85% of the total water depth. Fairly steep sloping walls do not influence the bifurcation mechanism. In addition, an elliptical horizontal cross section of the obstacle revealed that an important parameter for the bifurcation to occur is the length that the streamer has to travel around the obstacle and not the dimension of the obstacle in the direction orthogonal to the motion of the vortex, as expressed by Eq. (10).

In the present experiments, only two of the three parameters regulating the interaction of a vortex with an obstacle were varied. The two geometrical parameters, D/d and Y/R, determine the distance the streamer undergoes around the obstacle and ultimately the value of the Reynolds number of the streamer once it leaves the obstacle. As shown by C02, for bifurcation to occur the streamer must have a Reynolds number $400 \leq Re \leq 1100$. The novelty of the present work lies in determining how these two geometrical parameters are modified when the geometry of the obstacle deviates from a circular cylindrical island. However, a third relevant parameter is the relative strength of the vortex compared to the background rotation, i.e. the Rossby number $R_o = (\zeta/f)$. As mentioned in Section 5b, in the present experiments the value of the Rossby number was approximately constant $R_o \approx 0.6 - 1$. The technique used to generate the cyclonic vortex determined the strength of the vortex. The melting of the ice cube produced a dense plume and, hence, a low pressure with inward velocity toward it. In a rotating fluid, the Coriolis force deflects such inward velocities to give rise to the approximately geostrophic cyclonic vortex. The variation of the Rossby number over a few orders of magnitude is not a trivial task when using the laboratory experimental apparatus described in Section 2. In order to vary the vortex strength, the intensity of the dense plume (i.e. low pressure) has to be varied. Hence, withdrawing fluid using of a sink positioned on the sloping bottom (see Section 2) and varying the strength of the sink flow would be a more appropriate method to generate vortices with different strengths. Furthermore, the value of the Coriolis parameter could be changed. However, the present approach involves the manual positioning of an ice cube in the tank and renders high rotation rates of the table prohibitive. Hence, we decided to investigate first the dynamical importance and role of the two geometrical parameters, D/d and Y/R, using the simple experimental apparatus shown in Figure 1. The outcome of the experiments described in this paper showed such a richness in dynamics that we believe it is important to understand and report first before investigating the importance and effect of

a varying Rossby number. A future study, implementing a more sophisticated apparatus and a different technique to generate vortices, will investigate the importance of the Rossby number on the dynamics described in the present paper. We expect that variation of the Rossby number may modify, in particular, the behavior of the interaction of a vortex with a submersed obstacle discussed in Section 5b.

The theoretical approach described in Section 4a does not depend on the sign of the vortex; hence, the results obtained for a cyclonic vortex can be easily extended to an anticyclonic vortex (see Section 2a(ii)). Comparison with field observations indicates that processes similar to those observed in the laboratory took place and that the relevant nondimensional parameters discussed in the present paper give predictions in agreement with field observations. Finally, this study suggests that the interaction of meddies with seamounts could be an important mechanism for the Mediterranean salt tongue formation and maintenance, as also suggested by Wang and Dewar (2003). The idea that meddies slowly decay, surviving for a period of four to five years, and leave a dilute trail of salty and warm water in their wake (Käse and Zenk, 1987) is a possible one only if meddies remain clear of seamounts. The recent estimate (Richardson *et al.,* 2000) that 90% of meddies collide with major seamounts indicates that a more likely scenario is one in which meddies may inject stronger concentration of warm salty water locally in the vicinity of the seamounts, and possibly redistribute their signature into two vortices. These bifurcations will then enhance the redistribution of heat and salt in the North Atlantic, since a larger number of vortices will correspond to a larger number of dilute trails and a higher probability of vortex-seamount interaction. Presently, vortex parameterizations used in ocean models do not take into account this mechanism for redistribution of heat and salt. The model physics and parameterizations which generate and maintain the Mediterranean salt tongue are possibly inappropriate or inadequate without consideration of the dynamics of meddies interacting with seamounts.

Acknowledgments. We wish to thank Jason Hyatt and Joe Pedlosky for invaluable discussions, carefully reading drafts and substantially improving the clarity of the manuscript. Discussions with Bill Dewar were very helpful. Support was given by the National Science Foundation project number OCE-0081756. The laboratory experiments were carried out with the able assistance of Keith Bradley. This is WHOI contribution number 11034.

REFERENCES

Bower, A. S., L. Armi and I. Ambar. 1997. Lagrangian observation of meddy formation during a Mediterranean undercurrent seeding experiment. J. Phys. Oceanogr., *27,* 2545–2575.

Carnevale, G. F., R. C. Kloosterziel and G. J. F. van Heijst. 1991. Propagation of barotropic vortices over topography in a rotating tank. J. Fluid Mech., *233,* 119–139.

Cenedese, C. 2002. Laboratory experiments on mesoscale vortices colliding with a seamount. J. Geophys. Res., *107*(*C6*), 10.1029/2000JC000599.

Cenedese, C. and J. A. Whitehead. 2000. Eddy-shedding from a boundary current around a cape over a sloping bottom. J. Phys. Oceanogr., *30,* 1514–1531.

Cushman-Roisin, B. 1994. Introduction to Geophysical Fluid Dynamics, Prentice-Hall, 320 pp.

Dalziel, S. B. 1992. DigImage: System Overview, Cambridge Environmental Research Consultants, Ltd., 43 pp.

Dewar, W. K. 2002. Baroclinic eddy interaction with isolated topography. J. Phys. Oceanogr., *32,* 2789–2805.

Godfrey, J. S. 1989. A Sverdrup model of the depth-integrated flow from the world ocean allowing for island circulations. Geophys. Astrophys. Fluid Dyn., *45,* 89–112.

Herbette, S., Y. Morel and M. Arhan. 2003. Erosion of a surface vortex by a seamount. J. Phys. Oceanogr., *33,* 1664–1679.

Hide, R. and A. Ibbetson. 1966. An experimental study of "Taylor Columns." ICARUS, *5,* 279–290.

Käse, R. H. and W. Zenk. 1987. Reconstructed Mediterranean salt lens trajectories. J. Phys. Oceanogr., *17,* 158–163.

Kloosterziel, R. C. and G. J. F. van Heijst. 1991. An experimental study of unstable barotropic vortices in a rotating fluid. J. Fluid Mech., *223,* 1–24.

Linden, P. F., B. M. Boubnov and S. B. Dalziel. 1995. Source-sink turbulence in a rotating stratified fluid. J. Fluid Mech., *298,* 81–112.

Lucas, J. H. and D. Rockwell. 1988. Interaction of impulsively generated vortex pairs with bodies. J. Fluid Mech., *197,* 571–594.

McCartney, M. S. 1975. Inertial Taylor columns on a beta plane. J. Fluid Mech., *68,* 71–95.

Orlandi, P. 1993. Vortex dipoles impinging on circular cylinders. Phys. Fluids, *5,* 2196–2206.

Pedlosky, J., L. J. Pratt, M. A. Spall and K. R. Helfrich. 1997. Circulation around islands and ridges. J. Mar. Res., *55,* 1199–1251.

Richardson, P. L., A. S. Bower and W. Zenk. 2000. A census of meddies tracked by floats. Prog. Oceanogr., *45,* 209–250.

Richardson, P. L. and A. Tychensky. 1998. Meddy trajectories in the Canary Basin measured during the SEMAPHORE experiment, 1993–1995. J. Geophys. Res., *103,* 25029–25045.

Schwierz, C. B. and H. C. Davies. 2003. Evolution of a synoptic-scale vortex advecting toward a high mountain. Tellus, *55A,* 158–172.

Simmons, H. L. and D. Nof. 2000. Islands as eddy splitters. J. Mar. Res., *58,* 919–956.

Whitehead, J. A., M. E. Stern, G. R. Flierl and B. A. Klinger. 1990. Experimental observations of baroclinic eddies on a sloping bottom. J. Geophys. Res., *95,* 9585–9610.

Verzicco, R., J. B. Flor, G. J. F. van Heijst and P. Orlandi. 1995. Numerical and experimental study of the interaction between a vortex dipole and a circular cylinder. Expt. in Fluids, *18,* 153–163.

Voropayev, S. I. and Y. A. Afanasyev. 1994. Symmetric interaction of developing horizontal jet in a stratified fluid with a vertical cylinder. Phys. Fluids, *6,* 2032–2037.

Wang, G. and W. K. Dewar. 2003. Meddy-seamount interactions: Implications for the Mediterranean Salt Tongue. J. Phys. Oceanogr., *33,* 2446–2461.

Zhang, X., D. S. McGuinness and D. L. Boyer. 1994. Narrow barotropic currents impinging on an isolated seamount. J. Geophys. Res., *99,* 22707–22724.

Received: *4 March, 2004;* revised: *18 June, 2004.*